International Core Journal of Engineering Volume 11 Issue 10, 2025
ISSN: 2414-1895 DOI: 10.6919/ICJE.202510_11(10).0010

Research on Fault Diagnosis of UAV Acceleration Sensor based on GS-HPO-SVM

Zimo Li*

Nanjing Institute of Technology, Nanjing, Jiangsu, 211167, China

*Corresponding author's e-mail: cnLizimo@outlook.com

Abstract

All articles *must* contain an abstract. The abstract text should be formatted using 10 point Times or Times New Roman and indented 25 mm from the left margin. Leave 10 mm space after the abstract before you begin the main text of your article, starting on the same page as the abstract. The abstract should give readers concise information about the content of the article and indicate the main results obtained and conclusions drawn. The abstract is not part of the text and should be complete in itself; no table numbers, figure numbers, references or displayed mathematical expressions should be included. It should be suitable for direct inclusion in abstracting services and should not normally exceed 200 words in a single paragraph. Since contemporary information-retrieval systems rely heavily on the content of titles and abstracts to identify relevant articles in literature searches, great care should be taken in constructing both.

Keywords

Acceleration Sensor; Fault Diagnosis; Multi-domain Feature Extraction; Z-score Standardization; t-SNE Dimensionality Reduction; One-vs-All Encoding; Grid Search Hyperparameter Optimization; Support Vector Machine (SVM) Introduction.

1. Introduction

Recent advancements in UAV technology have expanded its applications across military operations, logistics, agricultural monitoring, aerial surveying, and emergency response, leveraging advantages such as high maneuverability, concealment, and cost-effectiveness. Acceleration sensors, critical for measuring multi-axis acceleration in UAVs, can induce erroneous attitude estimation and flight control failures upon malfunction, potentially causing severe accidents. Hence, enhancing the accuracy and speed of fault diagnosis is imperative. For instance, military operations require precise acceleration data for reconnaissance, target engagement, and surveillance; prompt fault diagnosis ensures mission continuity. Emergency response relies on high-speed UAV deployment, where sensor fault rates escalate under intense operational loads. Efficient diagnosis is vital for minimizing response time.

Existing research on acceleration sensor fault diagnosis and SVM optimization remains limited in UAV-specific contexts. Studies focus primarily on data feature processing and diagnostic modeling: *International work*: Schmidt et al. developed a ResCNN-BiLSTM hybrid model under 10dB noise [1]. Kumar et al. proposed an adaptive kernel parameter tuning framework for Support Vector Machines by integrating Genetic Algorithms and Particle Swarm Optimization [2]. Quantum-behaved Particle Swarm Optimization (QPSO) reduces SVM classification errors [3]. *Domestic work*: Median/wavelet filtering denoises sensor data [4]. Teaching-learning-based Grey Wolf Optimizer (TLGWO) self-tunes SVM parameters [5]. PCA-SVM hybrids improve dimensionality reduction [6]. Least Squares SVM (LS-SVM) enhances fault isolation efficiency [7].

ISSN: 2414-1895 DOI: 10.6919/ICJE.202510_11(10).0010

However, limitations persist:Inadequate feature extraction compromises model generalization. Methods like MiniCV may overlook global optima by non-exhaustive hyperparameter search. Native SVM's binary classification struggles with multiclass fault imbalance.

To address these gaps, this paper proposes a GS-HPO-SVM fault diagnosis model. Data from the ADXL326 sensor in DJI WooKong-M flight controllers undergo multi-domain feature extraction to clarify fault boundaries. A multiclass strategy resolves classification imbalance, while grid search ensures global hyperparameter optimization. Model efficacy is validated through comparative analysis.

2. Acceleration Sensor Signal Acquisition

This study focuses on the ADI ADXL326 acceleration sensor in DJI WooKong-M flight controllers, F which is critical for triaxial acceleration data acquisition, attitude estimation, and stabilization control. Fig. 1 shows signals acquired under normal conditions.

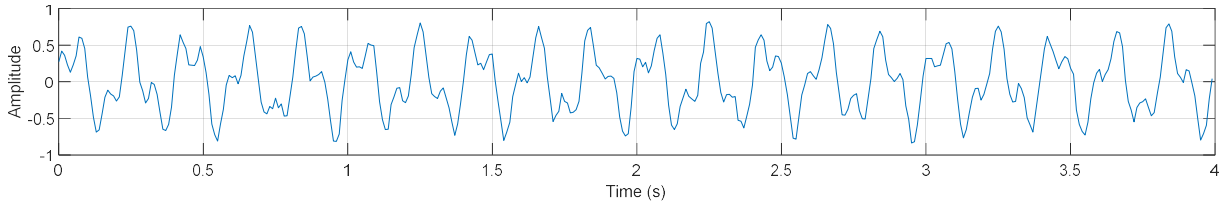

Fig. 1 Normal signals.

Under environmental stress (temperature/vibration/EMI) and mechanical fatigue, the sensor is prone to bias, noise, and drift faults. Bias faults manifest as sudden stepwise baseline shifts. Noise faults exhibit increased spikes and random amplitude mutations. Drift faults show linearly/quadratically increasing baselines with progressive center offsets. Figs 2(a), (b), and (c) display signals under bias, noise, and drift faults.

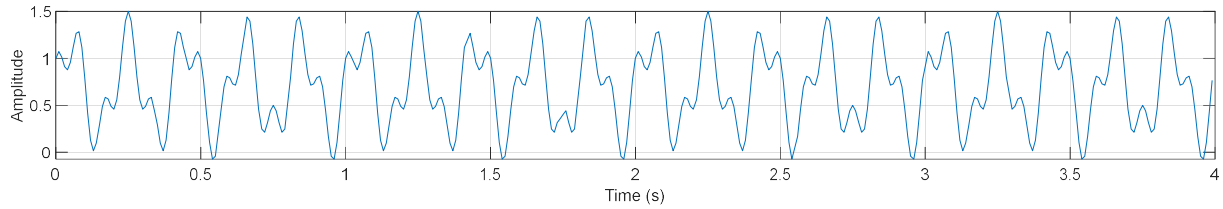

(a)Bias fault

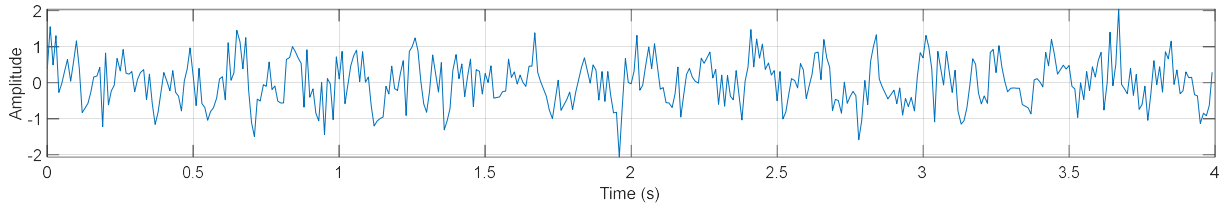

(b)Noise fault

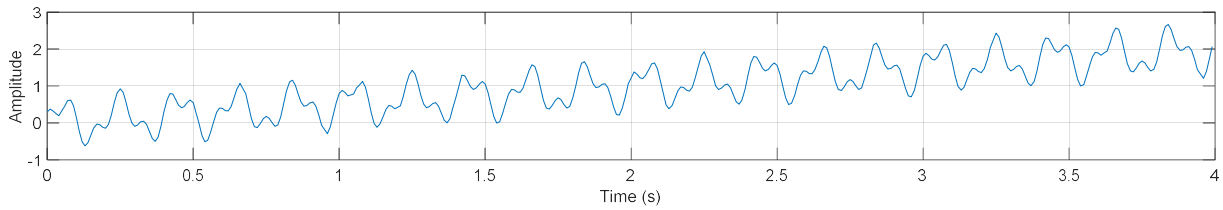

(c)Drift fault

Fig. 2 Fault signals.

ISSN: 2414-1895 DOI: 10.6919/ICJE.202510_11(10).0010

3. Multi-Domain Feature Extraction

To transform raw signals acquired from the acceleration sensor into discriminative information representations for fault modes, this study performs feature extraction across three domains: time domain, frequency domain, and time-frequency domain. The extracted features subsequently undergo Z-score standardization, t-SNE dimensionality reduction, and visualization to construct the input dataset for the SVM-based fault diagnosis model.

3.1 Time-Domain Features

Time-domain features are statistical properties analyzing signal variations over time, characterized by high real-time performance, computational simplicity, and transient sensitivity. Table 1 details the computational methods for time-domain features.

Table 1. Time-domain features.

Feature	Description
Mean	Signal average
STD	Deviation from mean
RMS	Average energy
Kurtosis	Distribution peakedness
Skewness	Distribution asymmetry
Peak Value	Maximum amplitude
Valley Value	Minimum amplitude
Peak-to-Peak	Dynamic range
Crest Factor	Peak/RMS ratio

3.2 Time-Domain Features

Frequency-domain features are statistics extracted after Fourier transform, characterized by noise robustness and direct correlation with fault characteristic frequencies. Table 2 details the computational methods for frequency-domain features.

Table 2. Frequency -domain features.

Feature	Description
Dominant Frequency	Strongest spectral component
Spectral Energy	Total frequency-domain energy
Spectral Entropy	Frequency component disorder

3.3 Time-Frequency Features

Time-frequency features combine time-frequency representations to reveal frequency component evolution, characterized by applicability to non-stationary signals and comprehensive time-varying dynamics characterization. Table 3 details the computational methods for time-frequency features.

Table 3. Time-Frequency features.

Feature	Description
Approximation Energy	Low-frequency energy (LL)
Detail 1 Energy	High-frequency energy (LH)
Detail 2 Energy	High-frequency energy (HL, HH)

3.4 Z-score Standardization

Z-score standardization transforms data to follow a standard normal distribution (mean=0, std=1), serving as a core preprocessing technique to enhance model performance and enable cross-feature

ISSN: 2414-1895 DOI: 10.6919/ICJE.202510_11(10).0010

comparison, particularly suited for distance/gradient-dependent algorithms like SVM. The calculation formula is:

$$z = \frac{x-\mu}{\sigma} \tag{1}$$

where x is a raw data point, μ is the dataset mean, and σ is the dataset standard deviation.

3.5 t-SNE Dimensionality Reduction and Visualization

t-SNE is a nonlinear manifold learning algorithm designed for low-dimensional embedding visualization of high-dimensional data. It defines conditional probability distributions in high- and low-dimensional spaces to quantify inter-sample similarities, minimizing the Kullback-Leibler divergence:

$$\text{Cost}=\min \sum_i \sum_j p_{j|i} \log \frac{p_{j|i}}{q_{ij}} \tag{2}$$

where $p_{j|i}$ is the high-dimensional conditional probability (Gaussian), and q_{ij} is the low-dimensional similarity (Student's t-distribution). Fig. 3 visualizes the feature distribution after t-SNE dimensionality reduction.

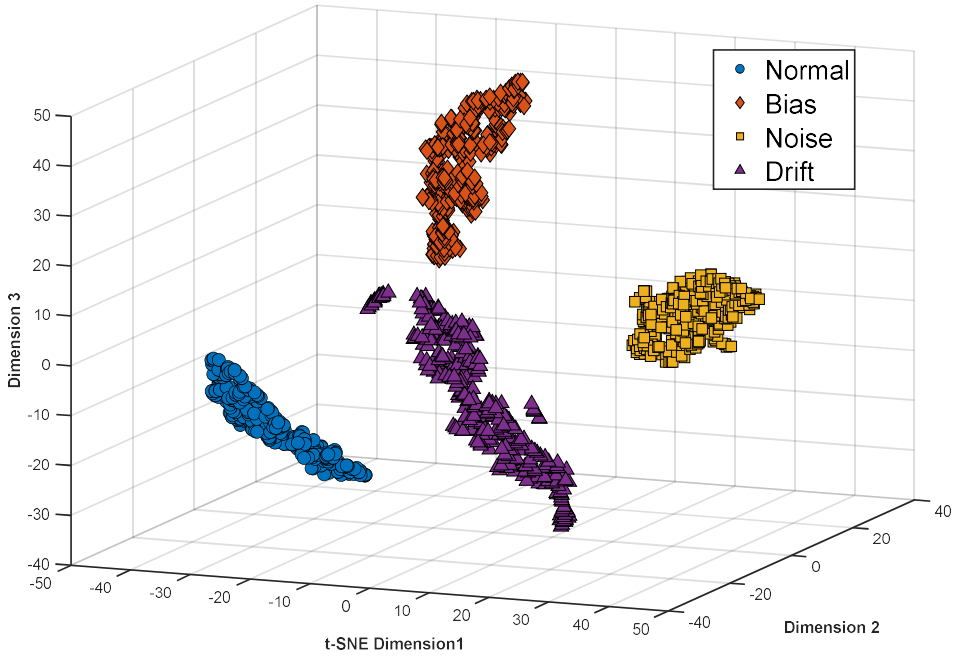

Fig. 3 t-SNE visualization of fault features.

4. GS-HPO-SVM Based Fault Diagnosis

4.1 SVM Model

Support Vector Machines (SVM) identify an optimal hyperplane to separate classes while maximizing the margin, with core principle being structural risk minimization to enhance generalization without compromising accuracy.

For linear classification, it seeks the maximum-margin hyperplane for linearly separable data.Given a sample set $\{(x_i, y_i)\}$, $y_i \in \{-1, +1\}$, the hyperplane equation is:

ISSN: 2414-1895 DOI: 10.6919/ICJE.202510_11(10).0010

$$w^T x + b = 0 \tag{3}$$

where $\mathbf{w}$ is the normal vector and b is the bias term.The margin is defined as:

$$Margin = \frac{2}{\|w\|} \tag{4}$$

The optimization minimizes$\|w\|$ subject to:

$$y_i(w^T x_i + b) \geq 1, \forall i \tag{5}$$

For nonlinear classification, kernel functions map data to higher dimensions for linear separability. Using kernel trick $\boldsymbol{\kappa(x_i, x_j)}$ without explicit high-dimensional computation:

$$f(x) = \text{sign}(\sum_{i=1}^{n} \alpha_i y_i \kappa(x_i^T, x) + b) \tag{6}$$

SVM offers advantages including high-dimensional efficiency, overfitting resistance, flexible nonlinear modeling, and noise/outlier robustness.

4.2 GS-HPO Model Optimization

Although standard SVM exhibits satisfactory performance, fault diagnosis requires higher efficiency without sacrificing accuracy; thus, this paper proposes GS-HPO optimized SVM to enhance diagnostic efficiency.The procedure is:

Step 1: Multiclass Strategy Design (One-vs-All Encoding)

Decompose the 4-class problem (normal/bias/noise/drift) into binary tasks, training one SVM classifier per category to resolve binary limitations and class imbalance.

Step 2: Hyperparameter Space Definition

Define key parameters and search ranges to establish a comprehensive hyperparameter optimization space.

Step 3: Grid Search Optimization

Grid search exhaustively evaluates all hyperparameter combinations to identify the performance-optimal configuration.Given hyperparameter set $\Theta = \{\theta_1, \theta_2, \ldots, \theta_k\}$ with discrete values $\theta_i \in V_i$, it constructs the Cartesian product space:

$$\Theta_{grid} = V_1 \times V_2 \times \cdots \times V_k \tag{7}$$

The optimization objective is:

$$\theta^* = \arg \max_{\theta \in \Theta_{grid}} \zeta(\theta) \tag{8}$$

where $\zeta(\theta)$ is the validation set performance metric.

For an SVM with m optimizable hyperparameters:

$$\Theta = \{C_1, C_2, \cdots, C_p\} \times \{\gamma_1, \gamma_2, \cdots, \gamma_q\} \times \{d_1, d_2, \cdots, d_r\} \times \kappa \tag{9}$$

ISSN: 2414-1895 DOI: 10.6919/ICJE.202510_11(10).0010

with kernel space $\kappa = \{linear, RBF, poynomial\}$ and $|\Theta| = p \times q \times r \times |\kappa| = 4 \times 3 \times 4 \times 3 = 144$

For each combination $\theta^{(i)}$, train model $f_{\theta^{(i)}}$ and compute:

$$\zeta(\theta^{(i)}) = \frac{1}{N_{val}} \sum_{j=1}^{N_{val}} \mathbb{I}\left(f_{\theta^{(i)}}(x_j) = y_j\right) \tag{10}$$

where $\mathbb{I}(\cdot)$ is the indicator function and N_{val} is the validation set size.

Grid search satisfies the global optimality condition:

$$\mathbb{P}\left(\zeta(\theta^{(i)}) \geq \zeta(\theta), \forall \theta \in \Theta_{grid}\right) = 1 \tag{11}$$

This guarantees complete traversal without overlooking superior solutions due to discrete finiteness. Grid search yields the global optimum $\theta^* = (\kappa = linear, C = 1)$, achieving optimal SVM performance. Fig. 4 shows the GS-HPO-SVM workflow, and Fig. 5 compares performance before/after optimization.

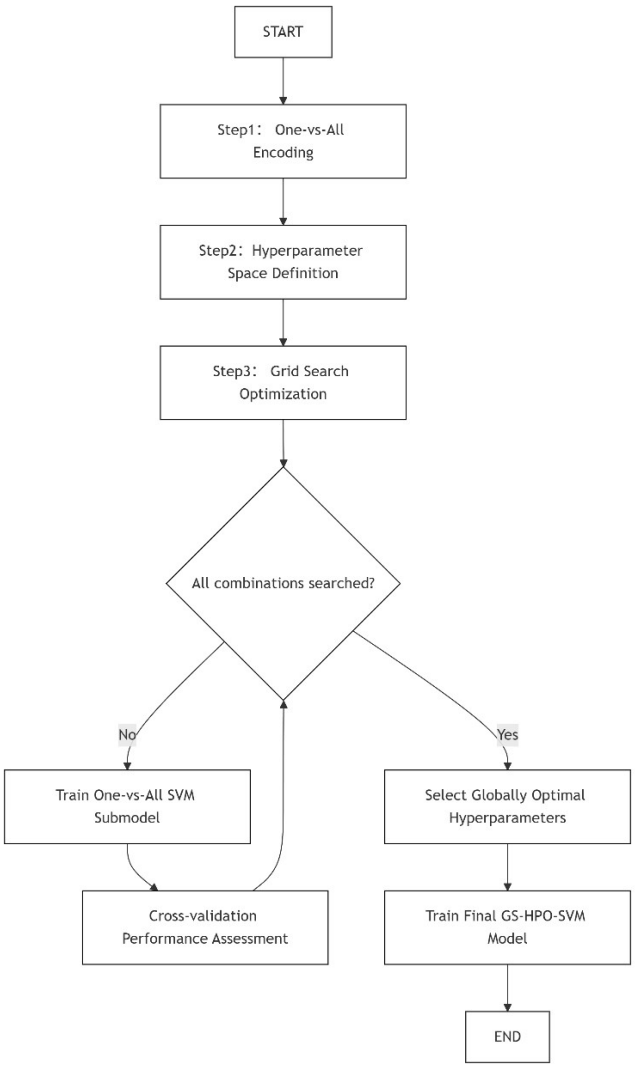

Fig. 4 GS-HPO-SVM algorithm workflow.

ISSN: 2414-1895 DOI: 10.6919/ICJE.202510_11(10).0010

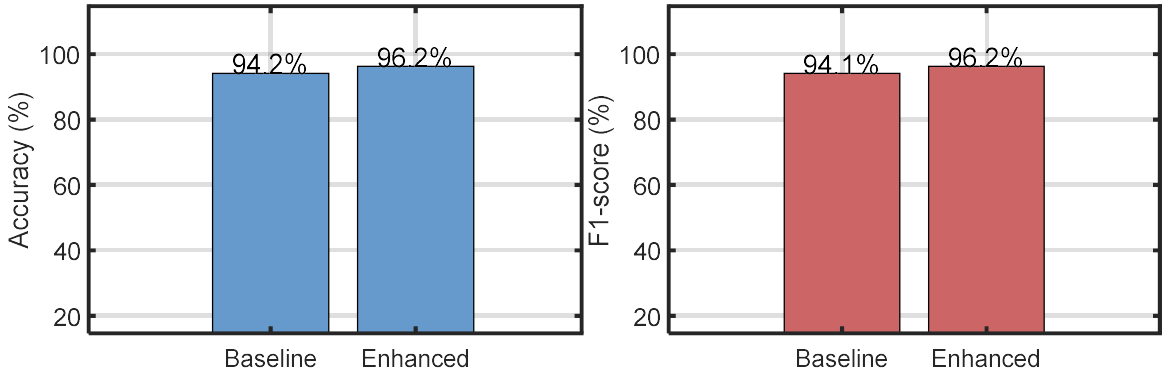

Fig. 5 Accuracy/F1-score before/after GS-HPO optimization.

4.3 GS-HPO-SVM based Fault Diagnosis

The GS-HPO-SVM fault diagnosis operates in five stages: Stage 1: Extract 15D features from time/frequency/time-frequency domains, apply Z-score and t-SNE to obtain feature vectors. Stage 2: Define classes (normal, bias, noise, drift) and partition data into 70% training, 15% testing, 15% validation.Stage 3: Construct SVM with One-vs-All strategy, apply GS-HPO for parameter optimization, and train the classifier. Stage 4: Evaluate the model on test and validation sets. Stage 5: Determine fault categories and analyze real-time results. Fig. 6 shows the diagnosis flowchart.

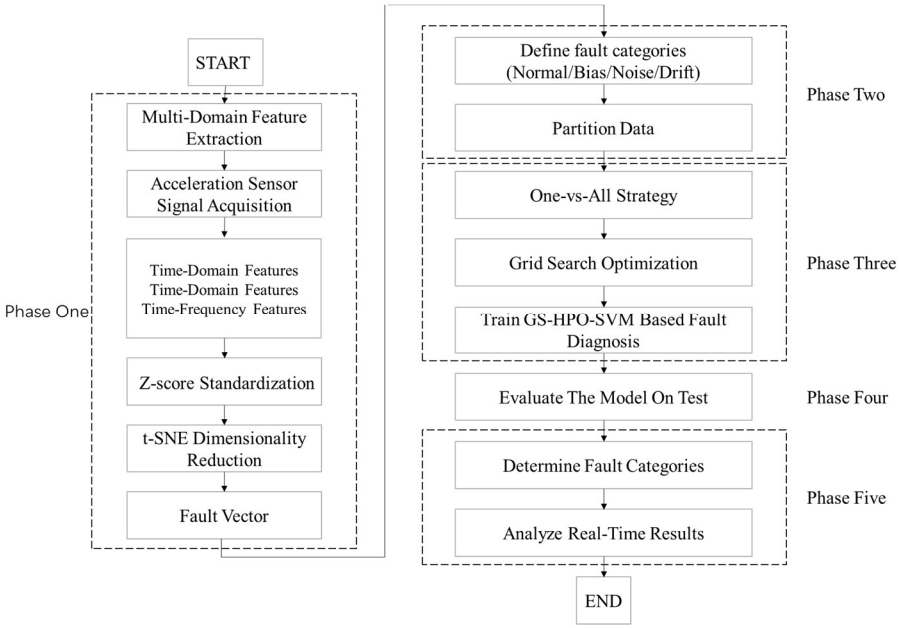

Fig. 6 GS-HPO-SVM fault diagnosis workflow.

5. Real-Time Diagnosis Results and Analysis

For normal, bias, noise, and drift states, 400 samples per state were collected (total 1,600 samples). Samples were partitioned into 70% training (1,120), 15% testing (240), and 15% validation (240) sets for fault classification. Cross-validation mitigated randomness-related overfitting through multiple training/validation cycles. Fig. 7 shows real-time diagnosis performance under GS-HPO-SVM. Comparisons with Decision Tree (DT) and Neural Network (NN) validate GS-HPO-SVM superiority (Fig. 8).

ISSN: 2414-1895 DOI: 10.6919/ICJE.202510_11(10).0010

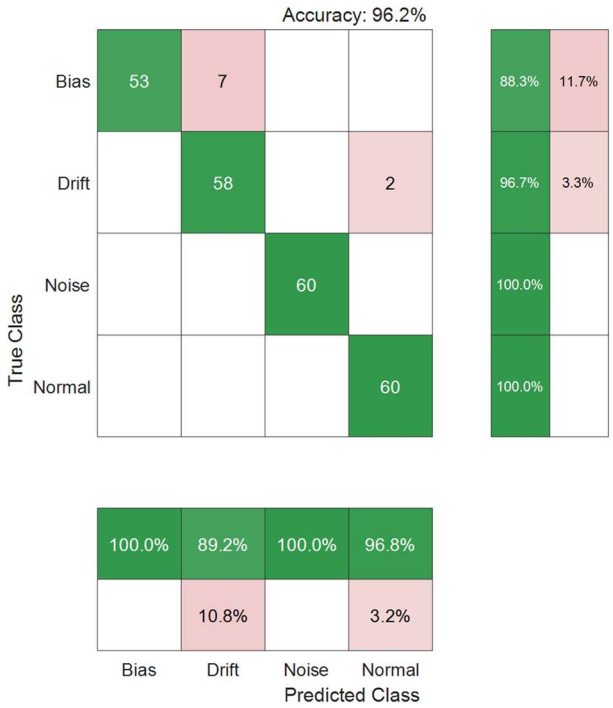

Fig. 7 Confusion matrix of GS-HPO-SVM model.

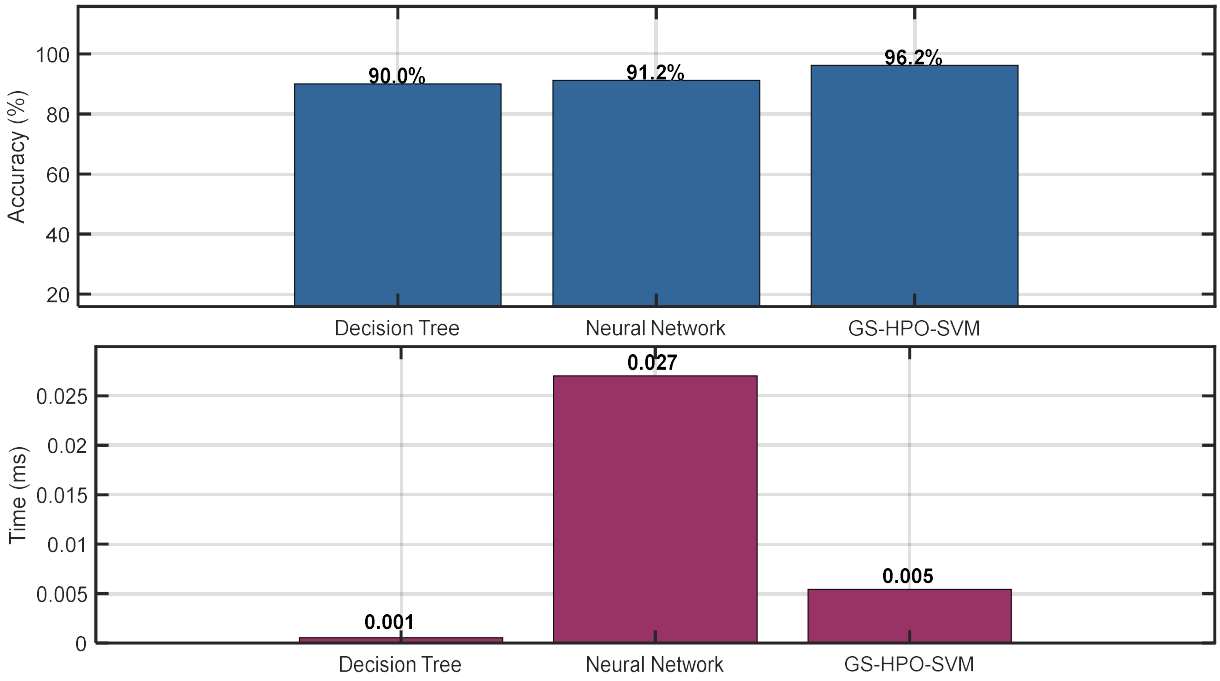

Fig. 8 Performance comparison with DT and NN models.

GS-HPO-SVM ranks first in accuracy and second in per-sample response time among the three algorithms, with response time 75% slower than DT but 225% faster than NN. This demonstrates GS-HPO-SVM's superior performance in balancing high accuracy and efficiency.

6. Conclusion

Addressing challenges of blurred fault boundaries, high-dimensional data complexity, and suboptimal model performance, this paper proposed an SVM fault diagnosis model with multi-domain feature extraction, multiclass strategy, and GS-HPO optimization. Multi-domain feature fusion with normalization and dimensionality reduction yields distinct, separable fault information. Multiclass

ISSN: 2414-1895 DOI: 10.6919/ICJE.202510_11(10).0010

strategy resolves SVM's binary limitation and class imbalance. GS-HPO enhances global optimum discovery, significantly improving accuracy and real-time performance.

Although only 1,600 samples were used, diagnostic results and comparative analysis confirm GS-HPO-SVM's significant advantages. The algorithm holds broad application prospects, warranting validation with larger datasets in future work.

References

[1] Schmidt, J., Müller, R., Braun, T. (2023) Deep Residual CNN-LSTM for Multi-Type Fault Diagnosis in Industrial Accelerometers. Mechanical Systems and Signal Processing, 189: 110081–110096.

[2] Kumar, A., Kim, J., Lyu, X. (2023) Adaptive Kernel Parameter Optimization for Support Vector Machines Using Metaheuristic Algorithms. IEEE Transactions on Pattern Analysis and Machine Intelligence, 45: 10235–10252.

[3] Tharwat, A., Hassanien, A.E. (2019) Quantum-Behaved Particle Swarm Optimization for Parameter Optimization of Support Vector Machine. J Classif ,36:576-598.

[4] Qiang M.H., Guo J. (2021) Research on Data Preprocessing Method for UAV Sensor Fault Diagnosis System. Ship Electronic Engineering, 41: 132-136.

[5] Li J., Chen J., Xiao C., et al. (2024) Fault Diagnosis of Fiber Bragg Grating Sensors Based on TLGWO-SVM. Journal of Wuhan University of Technology, 46: 129-136.

[6] Ma Y.J., Feng Y., Sun P.W., et al. (2024) Sensor Fault Diagnosis for Small Natural Circulation Lead-Cooled Fast Reactor Based on PCA-SVM. Nuclear Science and Engineering, 44: 464-471.

[7] Gao Y.H., Zhao D., Li Y.B. (2014) Fault Diagnosis of Small UAV Sensors Based on LSSVM and PCA. Fire Control & Command Control, 39: 111-114.